




Pore-Scale Evaluation of Physicochemical Interactions by Engineered Water Injections

Artur Shapoval¹ · Aleksandr Zhuravljov² · Zakhar Lanetc¹ · Sheikh S. Rahman¹ 

Received: 28 May 2022 / Accepted: 15 May 2023 / Published online: 31 May 2023
© Crown 2023

Abstract

Engineered water injections have gained a lot of interest as an economic and effective method of improving the oil recovery. However, the complexity of the physicochemical interactions between the brines of various compositions, oil and rock has led researchers to provide multiple ways to explain this phenomenon. In this work, we evaluate the previously suggested mechanisms, namely wettability alteration and emulsification, against high-resolution micro-CT coreflood observations in a limestone sample. This is achieved by integrating the effects of above-mentioned mechanisms into a volume-of-fluid simulation by using geochemical modelling and experimental measurements. This has allowed us to explain the effect of capillary force affecting mechanisms, whereby we were able to achieve 6% increase in recovery factor. We have also observed that these mechanisms have limitation in improving recovery due to fingering and subsequent formation of the stagnation zones inside the core samples. When viscous effect is considered in numerical study, 22% increase in recovery is achieved by reorientation of the main flow paths and mobilisation of the previously unconnected oil clusters. This result is closer to 24% increase in recovery factor which was observed in experimental study and signifies that viscosity increase due to emulsification is an important mechanism of engineered water injections.

Keywords Engineered waterfloods · Micro-CT · Pore scale · Enhanced oil recovery · Ion-tuned water

1 Introduction

Engineered water injections have become a much-discussed topic in the petroleum industry as an economic and sustainable method of increasing the oil recovery (Meng et al. 2015). Multiple reviews (Al-Shalabi and Sepehrnoori 2017; Awolayo et al. 2018; Hao et al. 2019) suggest that recovery can be enhanced by modifying both the overall salinity of the

✉ Sheikh S. Rahman
sheik.rahman@unsw.edu.au

¹ School of Minerals and Energy Resources Engineering, University of New South Wales, Kensington 2033, Australia

² Center of Innovation for Flow Through Porous Media, University of Wyoming, Wyoming 82071, USA

seawater and the composition of the potential determining ions (PDI) individually. For carbonate rocks, these PDI include Ca^{2+} , Mg^{2+} , SO_4^{2-} (Ding et al. 2019).

Based on the spontaneous imbibition and sessile drop contact angle studies, researchers have shown that wettability alteration by low-salinity or ion-tuned waters is a mechanism that significantly contributes to increase in oil recovery in ex situ and in situ studies (Selem et al. 2021; Shirazi et al. 2020; Zhang et al. 2007). However, as the number of studies on the topic grew (Bartels et al. 2019), inconsistencies in the evaluation of wettability change and oil recovery have been identified. This led the scientific community to develop additional methodologies to evaluate other potential mechanisms contributing to the efficiency of engineered waterfloods. Specifically, Masalmeh et al. (2019) have shown that the formation of in situ emulsion at the interface of oil and water is dependent on the oil composition and salinity of the injected water. Other studies (Shapoval et al. 2022; Tetteh et al. 2021; Unsal et al. 2019) have shown that the volume of generated emulsion is also controlled by the ionic composition of the water and can be observed and quantified using microtomography. Therefore, in situ formation of emulsion is another mechanism which provides an additional effect of engineered waterfloods. This is due primarily to the fact that emulsions increase the viscosity and interfacial tension at the interface as well as redirect water by blocking large pores, therefore reducing the fingering effects (McAuliffe 1973a; Unsal et al. 2016).

These foregoing complexities have made it difficult to model the governing mechanisms and predict the recovery. Majority of early modelling studies on the topic were focused on wettability change with two distinct geochemical approaches. The first approach is based on Bond Product Sum (BPS) (Brady et al. 2015), which is a summation of products of surface concentrations of opposite ions on oil and mineral. If all the species are negatively charged, BPS would be zero, species would not be electrostatically attracted to one another, and therefore, the surface is considered strong water wet. If both positively and negatively charged surface species are present, BPS would be high, and the wettability will move towards more oil-wet. The second approach, which has received a greater attention, is DLVO (Derjaguin–Landau–Verwey–Overbeek theory of colloidal stability)-based calculation (Derjaguin et al. 1987). In this approach, the attractive–repulsive microscopic forces between a surface and colloid (in this context rock surface and oil particle) are described by a disjoining pressure. Hirasaki (1991) has provided a significant extension to this theory in the context of oil recovery by developing a model for contact angle based on the disjoining pressure. As such, this approach allows to precisely predict specific contact angle values by knowing the chemistry of the injected brine, oil and rock mineralogy (Sanaei et al. 2019). At this moment, there is a lack of clear approach for modelling the fluid–fluid interactions with exception of some early works considering the effect in simple geometries with no experimental validation (Alizadeh et al. 2021).

There are two main direct numerical (DNS) approaches that are frequently applied to simulate multiphase flow on a pore scale: volume of fluid (VOF) and a number of multiphase extensions of lattice Boltzmann method (LBM) (e.g. Rothman–Keller, Shan–Chen, free energy models) (Huang et al. 2007; Lanetc et al. 2022; Vogel et al. 2005). In LBM, such simulation parameters such as viscosity, adhesion and cohesion forces depend on a voxel size and time-step values (Krüger et al. 2017). Thus, the usage of realistic parameters may lead to unfeasibly large number of time steps or computationally expensive mesh refinement. In turn, flow parameters can be set arbitrary for the VOF method which is based on the Navier–Stokes equation (Deshpande et al. 2012). However, the employability of the VOF method is still restricted by high computational costs when a large 3D geometry is considered. This issue can be addressed by the employment of relevant image-based

modelling (IBM) tools including grid coarsening and by parallel computing (Carrillo et al. 2022; Raeini et al. 2014). Shams et al. and Frank et al. have shown that it is possible to precisely predict localised contact angles and capillary snapping within the scope of above-discussed limitations (Frank et al. 2018; Shams et al. 2021).

The engineered water injections have been extensively studied by both lattice Boltzmann (LB) and VOF methods (Namaee-Ghasemi et al. 2021). For instance, the wettability alteration due to the injection of low salinity water in 3D micro-CT images of sandstones was modelled by (Akai et al. 2020) with the usage of colour gradient LBM. Likewise, (Aziz et al. 2019) used a VOF method to analyse flow dynamics under wettability alteration on 2D synthetic images. Nevertheless, both studies only considered the wettability alteration by the linear functional dependence between the contact angle and ions local concentration while other mechanisms (e.g. interfacial tension change, viscoelastic effects and emulsion generation) were neglected.

The goal of this study is to provide an exhaustive modelling approach for numerically predicting the results of the engineered waterfloods. To achieve this, we combine the observations from pore-scale imaging of the ion-tuned injections with numerical models of individual mechanisms and then evaluate the significance of both rock–fluid and fluid interactions on oil recovery from carbonate samples. To the best of our knowledge, this is the first work that considers the modelling of multiple mechanisms and at the same time compares the results of these models with pore-scale experimental data.

2 Materials and Methods

2.1 Waterflooding Experiments

2.1.1 Rock and Fluids

Indiana Limestone was used as a representative carbonate sample, which is a well-characterised rock with relatively homogeneous mineralogy. A micro-plug with diameter of 5.9 mm was prepared to allow for high resolution of the CT image. Full list of its properties is provided in Table 1.

Three types of brines were used in this study. Firstly, a formation water (FW) represents a carbonate reservoir formation brine. For the secondary recovery, synthetic sea water (SW) was used (Ding and Rahman 2018; Yousef et al. 2011). For the tertiary recovery, ion-tuned water (ITW) was injected. Ionic modification was done by decreasing the Ca^{2+} concentration 4 times when compared to SW. Full list of brine properties is presented in Table 2.

Table 1 Indiana Limestone microplugs properties

Parameter	UoM	IL_6_c
Length	mm	14.14
Diameter	mm	5.9
Porosity	%	18
Permeability	mD	113

Table 2 Chemical composition of the brines

Ion/parameter	UoM	FW	SW	ITW
Ca	ppm	9250	650	163
Na	ppm	52,952	18,300	18,300
Mg	ppm	1446	2110	2110
SO ₄	ppm	–	4290	4290
Cl	ppm	102,722	32,399	31,534
K	ppm	744	–	–
Ionic strength	mol/L	3.183	1.073	1.039

Dead crude oil was used in this study with its original properties listed in Table 3. For the purpose of CT imaging, the oil was mixed at 1:1 proportion with 1-Iododecane. To assure the oil-wetting conditions after the ageing, the total acid number (TAN) of the mixture was adjusted to 1.5 mg KOH/g using the stearic acid (Song et al. 2020; Standnes and Austad 2000).

2.1.2 Sample Preparation and Waterflooding

Samples were first saturated for 10 days with FW and then injected with the oil mixture. Next, they were aged for 2 weeks at 80 °C and 200 psi to establish the initial oil-wet conditions. Finally, the 20 PV of SW was injected at secondary recovery stage, followed by 20 PV of ITW. All the injections were conducted at 0.5 cc/min flowrate (Shapoval et al. 2021). This flowrate was estimated based on the scaling coefficient proposed by Rapoport and Leas, (1953) to minimise capillary end effects:

$$S_c = L * \nu * \mu_w > 1 \quad (1)$$

where L is the core length (cm), ν is the flow velocity (cc/min), μ_w is the water viscosity (cP).

2.1.3 Image Processing

Images were acquired at the following stages: dry, after ageing, after seawater injection and after ion-tuned water injection. Images were first registered to each other and then segmented using the watershed algorithm (Scanziani et al. 2018). At last, contact angles were

Table 3 Crude oil properties

Parameter	UoM	Value
Saturates (S)	Wt%	73.84
Aromatics (A)	Wt%	18.39
Resins (R)	Wt%	7.71
Asphaltenes (A)	Wt%	0.06
Total acid number (TAN)	mg KOH/g	0.2
Total base number (TBN)	mg KOH/g	0.3
Viscosity	cP	2.79

analysed using the in situ contact angle calculation algorithm developed by AlRatrou et al. (2017). Experimental procedure is further summarised in Fig. 1.

2.2 Rock–Fluid Interactions Modelling

2.2.1 Contact Angle Calculation

Rock–fluid interactions, quantitatively expressed as contact angle, are governed by the surface forces at the water–rock and water–oil interfaces. The summation of these surface forces gives rise to disjoining pressure (see Eq. (2)), which governs the ability of rock surface to adsorb or desorb oil.

$$\Pi(h) = \Pi_{vdW}(h) + \Pi_{EDL}(h) + \Pi_S(h) \quad (2)$$

where Π —disjoining pressure, Π_{vdW} —van der Waals force, Π_{EDL} —electrical double-layer force, Π_S —structural force, h —water film thickness.

Hirasaki (1991) provided an analytical solution, which allows to use the calculated disjoining pressure for the prediction of the contact angle:

$$1 - \cos(\theta) = \frac{1}{\sigma} \left(- \int_{h_0}^{h_\infty} \Pi dh - h_0 \Pi(h_0) \right) \quad (3)$$

where θ —contact angle, σ —interfacial tension (IFT), h_0 —is a limiting film thickness.

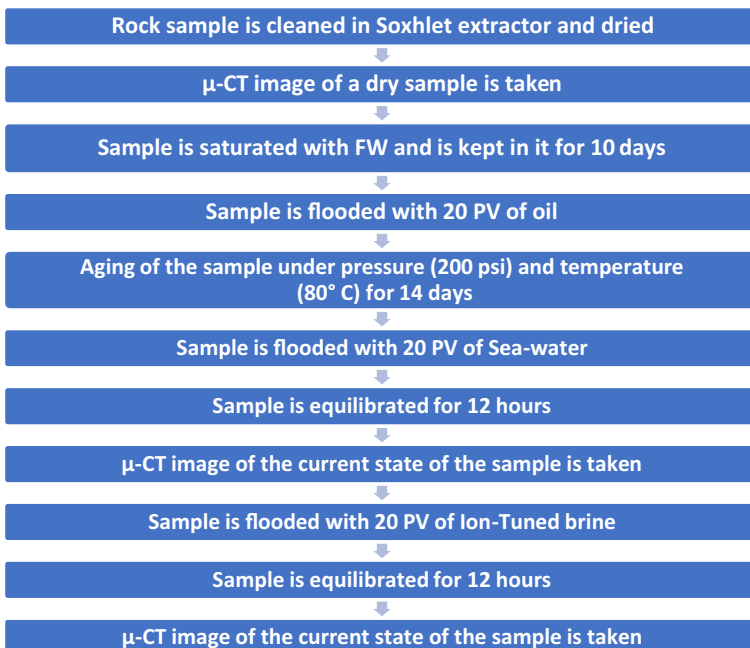


Fig. 1 Flowchart of the experimental procedure of core floods coupled with micro-CT imaging

It was previously discussed that disjoining pressure curve for calcitic rocks shows both positive and negative values (Jalili and Tabrizy 2014; Khurshid and Al-Shalabi 2022; Mahani et al. 2017; Maskari et al. 2020). At our conditions, disjoining pressure was estimated to be negative (see validation in Supporting Information), an assumption proposed by Hirasaki (1991), which states that the limiting film thickness is a thickness of a water molecule monolayer (0.3 nm), was used.

2.2.2 Surface Complexation Modelling

Out of the three forces that makeup the disjoining pressure, the electrical double-layer (EDL) force is the one that is controlled by the chemistry of the brine. Specifically, this force is based on the electrochemical interactions on the water–oil and water–rock interfaces. Numerically, EDL force is calculated as a linear solution of Poisson–Boltzmann equation (PBS) at a specific boundary condition. There are various conditions proposed in literature for fitting the experimental data; however, two mostly used methods include constant charge (CC) and constant potential (CP). In this work, we have used the constant potential boundary condition, which has been previously used to successfully model the EDL force for carbonates (Bordeaux-Rego et al. 2021; Sanaei et al. 2019):

$$\Pi_{EDL}(h) = n_b k_B T \left(\frac{2\psi_{r1}\psi_{r2} \cosh(kh) - \psi_{r1}^2 - \psi_{r2}^2}{(\sinh(kh))^2} \right) \quad (4)$$

where n_b —the ion density of the bulk solution, k_B —Boltzmann constant, 1.38×10^{-23} J/K, T —Temperature, 298 K, ψ_{ri} —reduced surface potential (see Eq. (5)), k —reciprocal Debye–Huckel length.

$$\psi_{ri} = \frac{e\zeta_i}{k_B T} \quad (5)$$

where e is elementary charge (1.6×10^{-19} C), ζ_i is the zeta potential.

As such, zeta potential is a parameter, which is required for estimating the contact angle and which is dependent on the ionic composition of the brine. Zeta potential can either be measured experimentally or modelled numerically using surface complexation modelling. Because the goal of this work is to maximise the modelling capabilities, we have used the surface complexation modelling (SCM) to predict the zeta potentials for various brines. Specifically, two SCMs were used to model the reactions between water and calcite and between water and oil, as described in Table 4.

For calcite, density of surface binding sites is assumed to be 4.95 sites/nm²; specific surface area is assumed to be 1 m²/g (Ding and Rahman 2018). For oil phase, site densities of carboxylate and nitrogen base groups were calculated using the following relationships:

$$c_{-COOH} = 0.602 \times 10^6 \frac{TAN}{1000a_{oil}MW_{KOH}} \quad (6)$$

$$c_{-NH} = 0.602 \times 10^6 \frac{TBN}{1000a_{oil}MW_{KOH}} \quad (7)$$

Table 4 Surface complexation model

Surface reaction	logK
<i>Calcite surface complexation model (after Ding and Rahman 2018; Qiao et al. 2015)</i>	
$>CO_3H = >CO_3^- + H^+$	-5.1
$>CO_3^- + Ca^{+2} = >CO_3Ca^+$	2.9
$>CO_3^- + Mg^{+2} = >CO_3Mg^+$	0.7
$>CaOH + H^+ = >CaOH^{+2}$	11.8
$>CaOH_2^+ + SO_4^{-2} = >CaSO_4^- + H_2O$	6.0
$>CaOH_2^+ + CO_3^{-2} = >CaCO_3^- + H_2O$	-2.1
<i>Oil surface complexation model (after Brady and Krumhansl 2012; Sanaei et al. 2019)</i>	
$>NH + H^+ = >NH_2^+$	6.0
$>COOH = >COO^- + H^+$	-4.7
$>COOH + Ca^{+2} = >COOCa^+ + H^+$	-3.8
$>COOH + Mg^{+2} = >COOMg^+ + H^+$	4.0

where 0.602×10^6 is a conversion from mol/m² to sites/m², α_{oil} is the specific surface area of oil (3.7 m²/g), MW_{KOH} is the molecular weight of potassium hydroxide in g/mol (Sanaei et al. 2019).

The results of the modelling and the contact angle calculations are presented in Fig. 2. The resulting contact angle distribution fits well to the average values identified by in situ contact angle measurements, as discussed in Sect. 3.1 Experimental data analysis.

2.3 Fluid–Fluid Interactions Modelling

The effect of fluid–fluid interactions is related to the formation of microemulsion at the interface between oil and water. Specifically, emulsification affects the flow of fluid by two mechanisms and was previously shown to be a mechanism of EOR by modified brine injections at pore scale (Masalmeh et al. 2019; Mohammadi et al. 2022).

Firstly, emulsion acts as an IFT decreasing agent. It is shown that modification of the water composition does not significantly affect the IFT between water and oil. However, the emulsions formed due to engineered water injections do have a low IFT towards both oil and water. As such, these emulsions can act as a low-IFT bridge, which allows to decrease the resisting

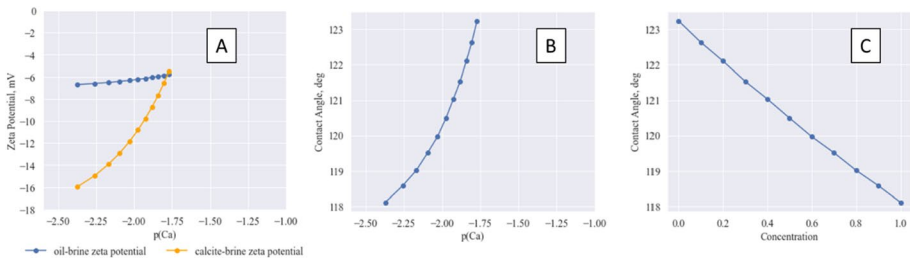


Fig. 2 Geochemical contact angle modelling relationships. **A** Zeta potential vs calcium concentration (blue—zeta potential for oil–water, orange—zeta potential for calcite water), **B** contact angle vs calcium concentration, **C** contact angle vs ITW concentration

capillary forces and improve the recovery. While it is not possible to completely reproduce the properties of in situ emulsions in laboratory environment, we have measured the IFT of various compositions of emulsions against seawater, as shown in Fig. 3. Experimental procedure is based on the works of (Mahani et al. 2015; McAuliffe 1973b) as follows: first a vial was filled with fluids of the ratio of interest, then emulsified and stabilised in the sonic bath for two hours. Then, the emulsified interface was extracted and IFT was measured using the pendant drop method (Drelich et al. 2002). Measurements were provided in the range of stable compositions. In this work, we assume that as the concentration of ion-tuned water reaches the water–oil interface, the IFT decreases. At 100% ion-tuned water, the concentration reaches the lowest measurable value (9.59 dyne/cm).

Secondly, emulsions have very high viscosity compared to oil. This allows to significantly improve the microscopic displacement efficiency due to improved mobility ratio. At laboratory conditions, the viscosity of oil–water emulsion (mixed at 1:1 ratio) was measured to be 573cP using the Brookfield DVII+ Cone/Plate viscometer (at 0.5 rpm to allow for the approximate representation of simulated shear rate). However, previous research has shown that the viscosity of emulsions can be as high as 2000 cP or even higher (Kokal and Al-Dokhi 2008; Umar et al. 2018). Therefore, in this study, the viscosity of the oil–ITW interface was used as a tuning parameter to compensate for history matching the microscopic recovery to that of the experimental subset.

2.4 Fluid Flow Modelling

In this section, a general mathematical description of the employed volume of fluid (VOF) method along with proposed modifications is provided. This approach was validated previously to provide highly precise description of the fluid–fluid interfaces in multiphase flow (Gamet et al. 2020; Li and Li 2018). The details of VOF methodology as well as its numerical representation and software implementation (InterFoam solver of OpenFoam CFD package) can be found in Deshpande et al. (2012).

While volume of fluid method is applied for two phase flow, it is based on a single phase form of governing CFD equations including the continuity equation and Navier–Stokes equation. The continuity equation can be expressed as follows:

$$\frac{\partial \rho}{\partial t} + \bar{\nabla} \cdot \rho \bar{v} = 0 \quad (8)$$

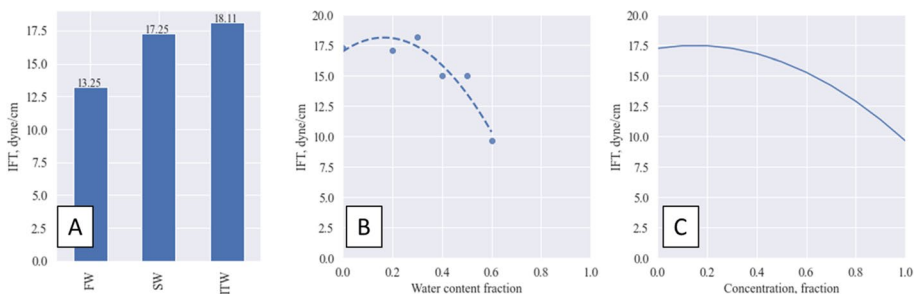


Fig. 3 Summary of IFT measurements and modelling. **A** IFT of pure brines vs crude oil. **B** IFT of emulsion vs the initial water fraction (reproduced from Shapoval et al. 2022), **C** scaled IFT of emulsion vs ITW concentration used in modelling

where biphasic phenomena are accounted throughout the averaged flow parameters of fluids' mixture such as density ($\rho = \alpha_w \rho_w + \alpha_o \rho_o$) and velocity (\bar{v}). Subscript indices w and o denote water and oil phases, correspondingly, while α is phase saturation. Navier–Stokes equation is employed in the same way as continuity equation above; however, it has additional factor (F_μ) for viscosity term and additional term responsible for capillarity:

$$\frac{\partial \rho \bar{v}}{\partial t} + \bar{\nabla} \cdot \rho \bar{v} \bar{v} = -\bar{\nabla} p + \bar{\nabla} \cdot F_\mu \mu \bar{\nabla} \bar{v} + \gamma \bar{\nabla} \cdot \bar{n}_{wo} \bar{\nabla} \alpha_w \tag{9}$$

where p is the pressure and μ is the average dynamic viscosity of fluids' mixture ($\mu = \alpha_w \mu_w + \alpha_o \mu_o$). The viscosity factor F_μ and interfacial tension γ both depend on concentration of ion-tuned water (C) for each of the grid blocks: $F_\mu = F_\mu(C)$ and $\gamma = \gamma(C)$. In turn, the equation which introduces the VOF advection scheme and provides the biphasic representation of the fluids' mixture is described with respect to the saturation of a particular phase:

$$\frac{\partial \alpha_w}{\partial t} + \bar{\nabla} \cdot \alpha_w \bar{v} + \bar{\nabla} \cdot \alpha_w (1 - \alpha_o) \bar{v}_r = 0 \tag{10}$$

where relative velocity (\bar{v}_r) is expressed as $\lambda \max(|\bar{v}|) \bar{n}_{wo}$, λ is numerical parameter responsible for interface compression and \bar{n}_{wo} is an average unit normal vector of the water–oil interface.

Since two kinds of water (sea water and ion-tuned water) are considered in this research, it is convenient to introduce governing equation for the concentration of ion-tuned water just after continuity equation:

$$\frac{\partial C}{\partial t} + \bar{v} \cdot \bar{\nabla} C = \bar{\nabla} \cdot D \bar{\nabla} C \tag{11}$$

where D is diffusivity coefficient. This transport equation is solved numerically using source code of conventional OpenFoam solver LaplacianFoam (Jasak et al. 2007).

To decrease the number of computational grid blocks in numerical meshes, a gradual local grid refinement is employed. A segmented micro-CT image is used for the generation of a Stereolithography (STL) image, which is then merged with a regular rectangular coarse mesh using SnappyHexMesh OpenFoam utility (Greenshields 2018). SnappyHexMesh is employed specifically to generate 3D and 2D meshes from segmented micro-CT images using hexahedra and split-hexahedra elements. The process refines and morphs the starting mesh, which should have grid blocks several times larger than the voxels of the initial micro-CT image, to closely approach the triangulated surface geometry through iterative procedures. This technique is particularly suitable for micro-CT based simulations due to its advantages, including smooth wall representation, internal connectivity preservation, reduced computational time and a lower grid block count. The SnappyHexMesh approach ensures smooth walls of porous void spaces, undistorted internal connectivity and automatic refinement of thin throats or bottlenecks in the micro-CT image, while preserving smooth wall transitions and a gradual change in the volumes of adjacent grid blocks. This combination of SnappyHexMesh and auxiliary functionality provides an efficient and suitable technique for micro-CT-based simulations.

Each simulation is carried out in three stages: primary injection of oil in a fully water-saturated sample, secondary injection of seawater and tertiary injection of the ion-tuned water. The following boundary conditions are imposed: velocity (inlet, based on the experimental value), pressure (outlet), no-flow (pore walls) and the contact angle are considered

dependent on the concentration of ITW and enforced as a boundary condition with respect to saturation. OpenFoam allows considering boundary conditions as dependent on an arbitrary volume field using an interpolation table. Such interpolation table is used to relate the contact angle dependence to the ITW concentration and, thus, account for wettability alteration. Two types of simulation datasets were used in this work: an Indiana Limestone subsection extracted from micro-CT image (uses experimental parameters as input) and a 2D synthetic heterogeneous porous media designed to conceptually replicate a carbonate rock due to a variety of geometries (uses synthetic set of parameters, see Table 5).

2.5 Assumptions

A number of assumptions related to the available experimental data and state of the art of numerical modelling are incorporated in this study. These assumptions are discussed, and an overview of the future directions of research on the topic is provided:

2.5.1 Effects of Microporosity and Surface Roughness

Due to the limitation of micro-CT imaging technology, especially when scanning of a fluid-saturated sample is considered, a specific subset of pores is observed to be below the voxel resolution of the image. As a result, these pores are excluded from the fine scale grid meshing of pore surface and two-phase numerical fluid flow analysis. Further development studies are, therefore, essential to integrate the volumetric and connectivity effects of multiphase flow and geochemical reactivity in these pores with fluids. Furthermore, it is not possible to consider certain features of rock matrix that include spatial connectivity of sub-resolution pores, surface roughness, etc. as discussed earlier within the workflow of image acquisition, segmentation and fine-scale meshing.

Table 5 Numerical simulation parameters

Parameter	Value (2D model)	Value (3D model)	Unit
Oil viscosity	2.79E−03	2.79E−03	Pa*s
Water viscosity	8.90E−04	8.90E−04	Pa*s
Viscosity ratio	3.13E+00	3.13E+00	
Oil density	8.33E+02	8.33E+02	kg/m ³
Water density	1.02E+03	1.02E+03	kg/m ³
Flowrate_3D	8.33E−08	8.33E−09	m ³ /sec
Velocity	2.95E−04	2.95E−04	m/sec
Capillary number	1.52E−05	1.52E−04	
Pressure at steady state	1.70E+05	1.70E+05	Pa
Contact angle SW	1.20E+02	1.23E+02	Deg
Contact angle ITW	7.50E+01	1.18E+02	Deg
Contact angle vs concentration function	Linear	See Fig. 2	
IFT SW	1.73E−02	1.73E−02	N/m
IFT ITW	1.70E−03	9.59E−03	N/m
IFT vs concentration function	Linear	see Fig. 3	
D	1.30E−09	1.30E−09	m ² /s

2.5.2 Spatial Distribution of Wettability

It is shown in section “Experimental data analysis” that the 3D image analysis has identified a range of contact angles within sub-section of the samples, importantly within both water-wet and oil-wet regions. An average measurement is used to represent the contact angle at the oil–water–rock interface to allow us model this contact angle change in the presence of different types and concentration of the brine at a specific time step. Further development work is essential for extracting local contact angles at the specific locations of the sample and their alteration due to injection of EOR fluids in the laboratory.

2.5.3 Ionic Species Diffusivity

Our model considers the transport of the ionic species through both the water and oil phases. First, the effect of DLVO forces in enhanced recovery is estimated mainly through the changes in the electrical double-layer force. As per DLVO theory, a constant water film is present along the surface of the rock. The more the initial oil-wetting condition—the thinner the water film. As the modified brine is injected into the sample, ionic transport occurs and brings the change in electrostatics between the three phases, thereby changing the thickness of this film and the corresponding contact angle (Ding and Rahman 2017; Myint and Firoozabadi 2015). The other consideration comes from the numerical procedure standpoint. The usage of diffusion concerning the entire pore volume allows accounting for the change of interfacial tension and contact angle on the walls where the two phases come together. Otherwise, these phenomena are not captured appropriately. Regarding the simulation studies, the flux magnitude due to diffusion is considerably smaller than the flux magnitude due to advection. Hence, it is reasonable to assume that the diffusion takes place in all phases.

It is important to note that the aim of this model is to simulate the coreflooding experiment, which is conventionally conducted to extract petrophysical data related to the EOR. In such experiment, advective transport has a higher magnitude of influence over the transport of the ionic species. As a result, all the mechanisms we propose are indeed limited to the zones near proximity of the oil–water interface at a given time during which experiments are conducted.

2.5.4 Kinetics of the Geochemistry

Kinetics of reactions is another important factor that was not fully considered in this study. In order to correctly characterise the timing of each mechanism in relation to the injection time, it requires further development studies. Continuum physics approach is a promising direction to provide the insights into the timescale of the modified water injection effects (Poisson–Boltzmann or Poisson–Nernst–Planck). This approach provides unique insight into ionic species diffusion and the dynamics of electrostatic interfaces (Pourakabarian et al. 2021, 2022).

2.5.5 Viscosity Reduction Dynamics

Dynamics of viscosity reduction due to emulsification by modified salinity waterflood is another unknown, which could not be incorporated due to lack of data. It was only recently

that both academia and industry have realised that fluid–fluid interactions are important and potentially key contributors to the EOR by modified waterfloods (Masalmeh et al. 2019; Tetteh et al. 2021). As such, one of the goals of this work is to provide clear pathways for more specialised research in future.

3 Results and Discussions

3.1 Experimental Data Analysis

A subset ($300 \times 300 \times 300$ voxels) of the micro-plug was analysed and used to validate the numerical model. Specifically, recovery factor and contact angle distributions were calculated after the secondary injection of the seawater as well as the tertiary injection of the ITW. The results of this analysis are presented in Fig. 4.

Experimental recovery data show that the recovery factor achieved by the seawater injection is 54%, while the recovery factor achieved after the tertiary injection of an ion-tuned water is 78%, with a total improvement of 24%. Wettability analysis confirms a change in wetting properties of the subsample towards more water wet, with the average contact angle across the sample after the seawater injection being 126 degrees (based on 26,800 measurements) and the average contact angle after the tertiary injection being 120 degrees (based on 24,468 measurements). The results show that the contact angle values are representative of the whole sample for which a detailed discussion is presented in previous study, see Shapoval et al. 2021.

3.2 Capillary Pressure Mechanisms Effects

In this section, we have first explored the effects of capillary-pressure affecting mechanisms, namely the contact angle reduction (attributed to rock–fluid interactions) and IFT reduction

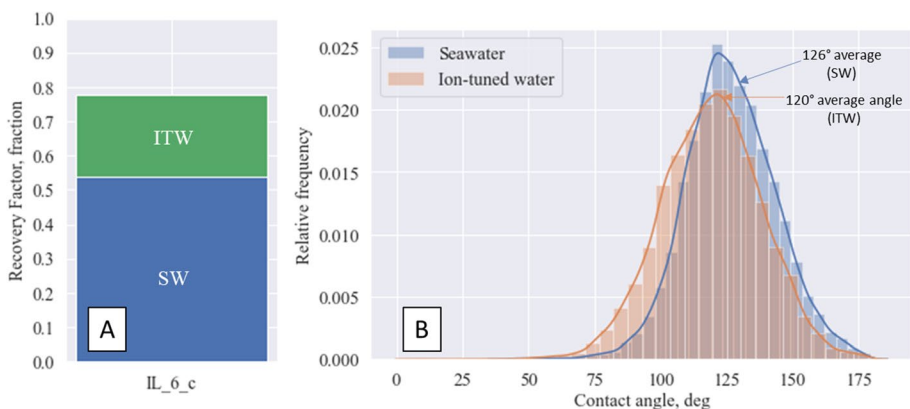


Fig. 4 Summary of the pore-scale analysis of a subset of experimental data. **A** Recovery factor, **B** in situ contact angle distribution

(attributed to fluid–fluid interactions). These mechanisms potentially improve the recovery by reducing the magnitude of the negative capillary force, as per the Young–Laplace Eq. (12):

$$P_c = -\frac{2\gamma\cos(\theta)}{r} \quad (12)$$

3.2.1 2D Synthetic Model

To allow for an explicit visualisation of the change of the capillary effect, first we have completed a simulation study using a synthetic model of a 1000×1000 voxel size. This model was completely saturated with water; after that, oil was injected to achieve irreducible water saturation. Next, seawater was injected until steady-state conditions were achieved. Finally, ITW was injected in a tertiary mode. In this case, a set of synthetic parameters was used, as presented in Table 5, which clearly demonstrate the effects of various forces related to ITW application on fluid flow and oil recovery.

The results of the tertiary injection in the 2D dataset are presented in Fig. 5. It becomes apparent from the figure that as soon as the shortest available flow path is established, the enhanced recovery becomes limited to the adjacent pores. Further, the additional recovery is assured only as the ion-tuned water spreads to the surface of the rock, at which point stagnated oil is mobilised.

A similar phenomenon was previously observed by Aziz et al., (2019), who have identified stagnant zones due to the established flow path as the main limitation of further recovery increases.

3.2.2 3D Indiana Limestone Model

The results of the modelling of capillary mechanisms in Indiana Limestone are presented in Fig. 6. It can be observed that the oil recovery is noticeably increased from the previously unconnected zones, proximity to the main flow path of the waterflood (Fig. 6A and B, examples of affected zones are highlighted in circles).

Quantitatively, it can be stated (see Fig. 6C) that recovery factor has increased by 6% from the secondary- (RF is 0.7) to tertiary recovery stage (RF is 0.76). However, this increase in recovery is lower than that observed in the experimental study (24%), in the same subsection of the micro-plug. This can be explained by the fact that this modelling approach accounted for only capillary effect (wettability alteration and IFT reduction) and ignored the viscous effect.

3.3 Combined Capillary and Viscous Mechanisms

The effect of the viscosity increase can be attributed to the change in the local capillary number of the porous media during the multiphase flow (see Eq. (13)). This phenomenon allows to redirect the main flow path of the fluid in the sample as the emulsion is being generated. As a result, oil recovery is increased even further by engaging the pores unaffected by the capillary pressure change.

$$N_{ca} = \frac{v\mu}{\gamma\cos(\theta)} \quad (13)$$

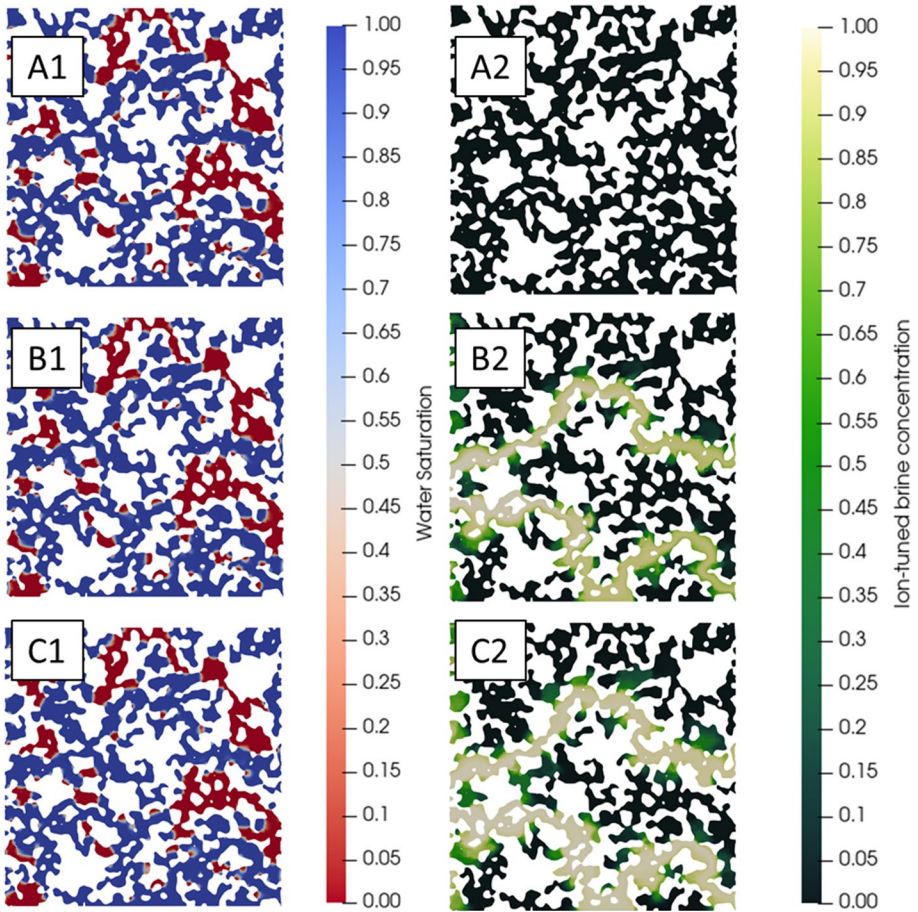


Fig. 5 Tertiary waterflooding simulation on synthetic 2d model using capillary pressure affecting mechanisms. **A1, B1, C1** Water saturation at 0, 0.45 and 1.35 s of injection. **A2, B2, C2** Ion-tuned brine concentration at 0, 0.45 and 1.35 s of injection

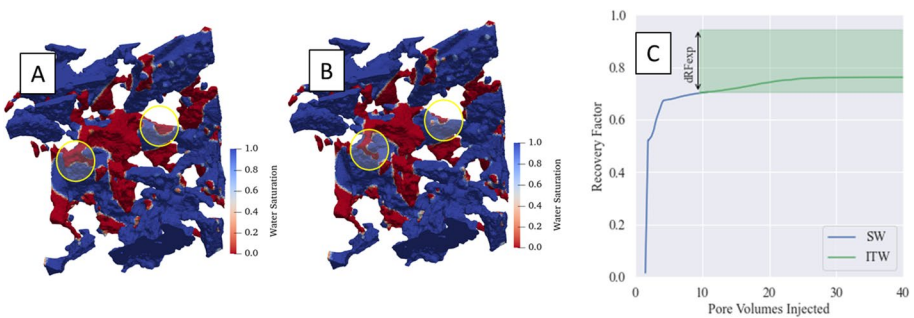


Fig. 6 Tertiary waterflooding simulation on Indiana Limestone sample using capillary pressure affecting mechanisms. **A** Saturation map after secondary recovery, **B** saturation map after tertiary recovery, **C** recovery factor vs pore volumes injected (green area shows the recovery enhancement measured experimentally from the same section of the sample)

3.3.1 2D Synthetic Model

In this case, we have explored the change in the flow behaviour due to increase in the viscosity (by 35 times to 97.65 cP), as presented in Fig. 7. One can observe that as the ITW front advances, the previously isolated pores are connected, thereby enabling oil to flow. When compared with the capillary mechanisms, these previously isolated pores away from the main flow path are now connected to the main flow path.

3.3.2 3D Indiana Limestone Model

The results of the combined model are presented in Fig. 8. It is observable that the additional oil recovery becomes more evenly distributed across the volume of the sample (Fig. 8A and B, examples of affected zones are highlighted in circles).

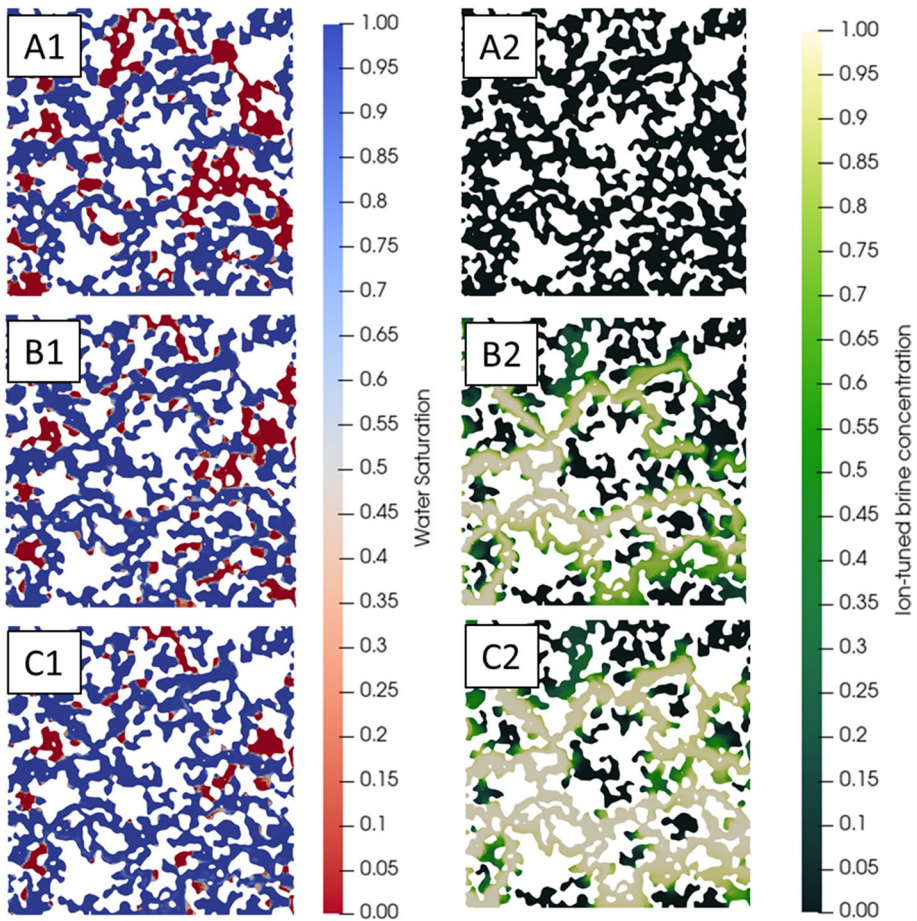


Fig. 7 Tertiary waterflooding simulation on synthetic 2d model using both viscous and capillary pressure altering mechanisms. **A1, B1, C1** Water saturation at 0, 0.45 and 1.35 s of injection. **A2, B2, C2** Ion-tuned brine concentration at 0, 0.45 and 1.35 s of injection

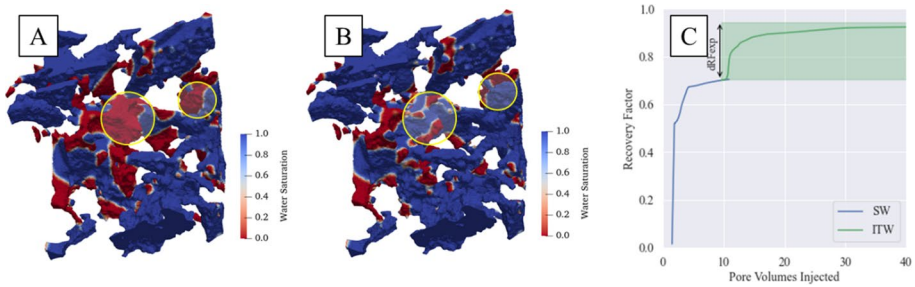


Fig. 8 Tertiary waterflooding simulation on Indiana Limestone sample using both viscous and capillary pressure altering mechanisms. **A** Saturation map after secondary recovery, **B** saturation map after tertiary recovery, **C** recovery factor vs pore volumes injected (green area shows the recovery enhancement measured experimentally from the same section of the sample)

Quantitatively (see Fig. 8C), when the capillary decrease and viscosity increase mechanism is combined, the recovery factor is improved from 0.70 to 0.92, with a total increase of 22%. This total recovery factor is reasonably close to the one observed in the experimental study (24%), which was achieved by increasing the viscosity of the ITW water–oil interface (by 35 times to 97.65cP). Notably, history matched viscosity is significantly lower than that indicative viscosity measured in the laboratory (97.65cP vs 573cP). This is related to the complexity of the formation of in situ emulsions during the fluid flow and other potential factors related to the ITW injections, which are outside of the scope of this work (time scale of wettability alteration, capillary number effect, calcite dissolution, pH change effect on IFT, etc.).

4 Conclusions

In this work, we have provided a set of models to represent the effect of engineered water injections and have compared the results of these models to the experimental data from a typical limestone. The results of this study can be summarised as follows:

- A numerical model was built to describe the three mechanisms of enhanced oil recovery by engineered waterfloods and grouped them into capillary force affecting (contact angle and IFT reduction) and viscous forces affecting (viscosity increase). Decrease in contact angle is explained by DLVO theory while IFT reduction and viscosity increase are explained by emulsification.
- Capillary force change due to ion-tuned water injection was proved to have an effect on oil recovery. However, when the capillary force is considered in the numerical model, the recovery factor achieved for the Indiana Limestone was significantly lower than that of the experiment.
- When the viscous force is considered in the numerical model, it was possible to match the experimental data of the Indiana Limestone, which significantly increased sweep efficiency and connectivity of previously isolated zones of the sample.
- Details of the implementation of ITW injection mechanisms can be further extended to include such components as the effect of pH change and dissolution–precipitation, which is important in the sub-porosity regions (Ansari et al. 2015; Kwak et al. 2018;

Yuan 2020). Likewise, the Darcy–Brinkman approach can be implemented for sub-resolution porosity inclusion in numerical simulations (Carrillo et al. 2020, 2022).

Appendix A: Surface Forces Calculation details

van der Waals force:

$$\Pi_{vdW}(h) = -\frac{A}{6\pi h^3} \quad (14)$$

where A is Hamaker constant and ranges from 0.3 to 10. For oil-wet surface, it is assumed to be 4.5×10^{-20} J and suitable for a water/oil/rock system (Habibi and Dehghanpour 2018; Hirasaki 1991; Visser 1972).

$$\Pi_{EDL}(h) = n_b k_B T \left(\frac{2\psi_{r1}\psi_{r2}\cosh(kh) - \psi_{r1}^2 - \psi_{r2}^2}{(\sinh(kh))^2} \right) \quad (15)$$

where n_b is the ion density of the bulk solution, k_B Boltzmann constant, 1.38×10^{-23} J/K, T —temperature, 298 K, ψ_{ri} —reduced surface potential, k —reciprocal Debye–Huckel length.

$$\psi_{ri} = \frac{e\zeta_i}{k_B T} \quad (16)$$

where e is elementary charge (1.6×10^{-19} C); ζ_i is the zeta potential in V.

Reciprocal Debye–Huckel length is given as:

$$k^{-1} = \sqrt{\frac{\epsilon_0 k_B \epsilon T}{2e^2 N_A I S}} \quad (17)$$

where ϵ_0 —permittivity of the free space, 8.85×10^{-12} C²/(Jm), ϵ —dielectric constant of water, 78.65, N_A —Avogadro's number, 6.022×10^{23} , $I S$ —ionic strength.

Structural force:

$$\Pi_S(h) = A_s e^{-\frac{h}{h_s}} \quad (18)$$

where A_s is a coefficient and h_s is a decay length. In this work, A_s is assumed to be 1.5×10^{10} Pa; h_s is assumed to be 0.05 nm (Hirasaki 1991).

Supplementary Information The online version contains supplementary material available at <https://doi.org/10.1007/s11242-023-01963-z>.

Acknowledgements The authors acknowledge the Tyree X-ray CT Facility, a UNSW network laboratory, funded by the UNSW Research Infrastructure Scheme, for the acquisition of the 3D μ XCT images.

Author Contributions AS conceptualised this study, provided the experimental work, geochemical modelling, numerical modelling data analysis and wrote the manuscript. AZ assisted with mathematical and software development and numerical modelling. ZL assisted with literature review and numerical modelling. SSR supervised the project with scientific input and reviewed the manuscript.

Funding Open Access funding enabled and organized by CAUL and its Member Institutions. The authors declare no sources of funding.

Declarations

Conflict of interest The authors declare that they have no conflict of interests.

Open Access This article is licensed under a Creative Commons Attribution 4.0 International License, which permits use, sharing, adaptation, distribution and reproduction in any medium or format, as long as you give appropriate credit to the original author(s) and the source, provide a link to the Creative Commons licence, and indicate if changes were made. The images or other third party material in this article are included in the article's Creative Commons licence, unless indicated otherwise in a credit line to the material. If material is not included in the article's Creative Commons licence and your intended use is not permitted by statutory regulation or exceeds the permitted use, you will need to obtain permission directly from the copyright holder. To view a copy of this licence, visit <http://creativecommons.org/licenses/by/4.0/>.

References

- Akai, T., Blunt, M.J., Bijeljic, B.: Pore-scale numerical simulation of low salinity water flooding using the lattice Boltzmann method. *J. Colloid Interface Sci.* **566**, 444–453 (2020). <https://doi.org/10.1016/j.jcis.2020.01.065>
- Alizadeh, M., Fatemi, M., Mousavi, M.: Direct numerical simulation of the effects of fluid/fluid and fluid/rock interactions on the oil displacement by low salinity and high salinity water: pore-scale occupancy and displacement mechanisms. *J. Petrol. Sci. Eng.* **196**, 107765 (2021). <https://doi.org/10.1016/j.petrol.2020.107765>
- AlRatrou, A., Raeini, A.Q., Bijeljic, B., Blunt, M.J.: Automatic measurement of contact angle in pore-space images. *Adv. Water Resour.* **109**, 158–169 (2017). <https://doi.org/10.1016/j.advwatres.2017.07.018>
- Al-Shalabi, E.W., Sepehrnoori, K.: Low salinity and engineered water injection for sandstones and carbonate reservoirs. Gulf Professional Publishing, Cambridge (2017)
- Ansari, A., Haroun, M., Rahman, M.M., Chilingar, G.V.: Electrokinetic driven low-concentration acid improved oil recovery in abu dhabi tight carbonate reservoirs. *Electrochimica Acta* **181**, 255–270 (2015). <https://doi.org/10.1016/j.electacta.2015.04.174>
- Awolayo, A., Sarma, H., Nghiem, L.: Brine-dependent recovery processes in carbonate and sandstone petroleum reservoirs: review of laboratory-field studies Interfacial mechanisms and modeling attempts. *Energies* **11**, 3020 (2018). <https://doi.org/10.3390/en11113020>
- Aziz, R., Joekar-Niasar, V., Martínez-Ferrer, P.J., Godinez-Brizuela, O.E., Theodoropoulos, C., Mahani, H.: Novel insights into pore-scale dynamics of wettability alteration during low salinity waterflooding. *Sci. Rep.* **9**, 9257 (2019). <https://doi.org/10.1038/s41598-019-45434-2>
- Bartels, W.-B., Mahani, H., Berg, S., Hassanizadeh, S.M.: Literature review of low salinity waterflooding from a length and time scale perspective. *Fuel* **236**, 338–353 (2019). <https://doi.org/10.1016/j.fuel.2018.09.018>
- Bordeaux-Rego, F., Mehrabi, M., Sanaei, A., Sepehrnoori, K.: Improvements on modelling wettability alteration by Engineered water injection: surface complexation at the oil/brine/rock contact. *Fuel* **284**, 118991 (2021). <https://doi.org/10.1016/j.fuel.2020.118991>
- Brady, P.V., Morrow, N.R., Fogden, A., Deniz, V., Loahardjo, N., Winoto, 2015. Electrostatics and the Low Salinity Effect in Sandstone Reservoirs. *Energy Fuels* **29**, 666–677. <https://doi.org/10.1021/ef502474a>
- Brady, P.V., Krumhansl, J.L.: A surface complexation model of oil–brine–sandstone interfaces at 100 °C: low salinity waterflooding. *J. Petrol. Sci. Eng.* **81**, 171–176 (2012). <https://doi.org/10.1016/j.petrol.2011.12.020>
- Carrillo, F.J., Bourg, I.C., Soullaine, C.: Multiphase flow modeling in multiscale porous media: an open-source micro-continuum approach. *J. Comput. Phys. X* **8**, 100073 (2020). <https://doi.org/10.1016/j.jcp.2020.100073>
- Carrillo, F.J., Soullaine, C., Bourg, I.C.: The impact of sub-resolution porosity on numerical simulations of multiphase flow. *Adv. Water Resour.* **161**, 104094 (2022). <https://doi.org/10.1016/j.advwatres.2021.104094>
- Derjaguin, B.V., Churaev, N.V., Muller, V.M.: The Derjaguin—Landau—Verwey—Overbeek (DLVO) theory of stability of lyophobic colloids. In: Derjaguin, B.V., Churaev, N.V., Muller, V.M. (eds.) *Surface Forces*, pp. 293–310. Springer, Boston (1987). https://doi.org/10.1007/978-1-4757-6639-4_8

- Deshpande, S.S., Anumolu, L., Trujillo, M.F.: Evaluating the performance of the two-phase flow solver interFoam. *Comput Sci Disc* **5**, 014016 (2012). <https://doi.org/10.1088/1749-4699/5/1/014016>
- Ding, H., Rahman, S.: Experimental and theoretical study of wettability alteration during low salinity water flooding—an state of the art review. *Colloids Surf., A* **520**, 622–639 (2017). <https://doi.org/10.1016/j.colsurfa.2017.02.006>
- Ding, H., Rahman, S.R.: Investigation of the impact of potential determining ions from surface complexation modeling. *Energy Fuels* **32**, 9314–9321 (2018). <https://doi.org/10.1021/acs.energyfuels.8b02131>
- Ding, H., Wang, Y., Shapoval, A., Zhao, Y., Rahman, S.S.: Macro- and microscopic study of “smart water” flooding in carbonate rocks—an image-based wettability examination. *Energy & Fuels* (2019). <https://doi.org/10.1021/acs.energyfuels.9b00638>
- Drelich, J., Fang, C., White, C.L.: Measurement of interfacial tension in fluid-fluid systems. In: *Encyclopedia of surface and colloid science*, pp. 3152–3166. Marcel Dekker Inc., New York city (2002)
- Frank, F., Liu, C., Scanziani, A., Alpak, F.O., Riviere, B.: An energy-based equilibrium contact angle boundary condition on jagged surfaces for phase-field methods. *J. Colloid Interface Sci.* **523**, 282–291 (2018). <https://doi.org/10.1016/j.jcis.2018.02.075>
- Gamet, L., Scala, M., Roenby, J., Scheufler, H., Pierson, J.-L.: Validation of volume-of-fluid OpenFOAM® isoAdvector solvers using single bubble benchmarks. *Computers & Fluids* **213**, 104722 (2020). <https://doi.org/10.1016/j.compfluid.2020.104722>
- Greenshields, C.J., 2018. Openfoam user guide version 6. The OpenFOAM foundation
- Habibi, A., Dehghanpour, H.: Wetting behavior of tight rocks: from core scale to pore scale. *Water Resour. Res.* **54**, 9162–9186 (2018). <https://doi.org/10.1029/2018WR023233>
- Hao, J., Mohammadkhani, S., Shahverdi, H., Eshfahany, M.N., Shapiro, A.: Mechanisms of smart waterflooding in carbonate oil reservoirs - a review. *J. Petrol. Sci. Eng.* **179**, 276–291 (2019). <https://doi.org/10.1016/j.petrol.2019.04.049>
- Hirasaki, G.J.: Wettability: fundamentals and surface forces. *SPE Form. Eval.* **6**, 217–226 (1991). <https://doi.org/10.2118/17367-PA>
- Huang, H., Thorne, D.T., Schaap, M.G., Sukop, M.C.: Proposed approximation for contact angles in Shan-and-Chen-type multicomponent multiphase lattice Boltzmann models. *Phys. Rev. E* **76**, 066701 (2007). <https://doi.org/10.1103/PhysRevE.76.066701>
- Jalili, Z., Tabrizy, V.A.: Mechanistic study of the wettability modification in carbonate and sandstone reservoirs during water/low salinity water flooding. *Energy Environ Res* (2014). <https://doi.org/10.5539/eer.v4n3p78r>
- Jasak, H., Jemcov, A., Kingdom, U., 2007. OpenFOAM: A C++ Library for Complex Physics Simulations, in: *International Workshop on Coupled Methods in Numerical Dynamics*, IUC. pp. 1–20.
- Khurshid, I., Al-Shalabi, E.W.: New insights into modeling disjoining pressure and wettability alteration by engineered water: surface complexation based rock composition study. *J. Petrol. Sci. Eng.* **208**, 109584 (2022). <https://doi.org/10.1016/j.petrol.2021.109584>
- Kokal, S., Al-Dokhi, M.: Case studies of emulsion behavior at reservoir conditions. *SPE Prod & Oper* **23**, 312–317 (2008). <https://doi.org/10.2118/105534-PA>
- Krüger, T., Kusumaatmaja, H., Kuzmin, A., Shardt, O., Silva, G., Viggén, E.M.: Multiphase and multicomponent flows. In: Krüger, T., Kusumaatmaja, H., Kuzmin, A., Shardt, O., Silva, G., Viggén, E.M. (eds.) *The Lattice Boltzmann method: principles and practice*, pp. 331–405. Springer, Cham (2017). https://doi.org/10.1007/978-3-319-44649-3_9
- Kwak, D., Han, S., Han, J., Wang, J., Lee, J., Lee, Y.: An experimental study on the pore characteristics alteration of carbonate during waterflooding. *J. Petrol. Sci. Eng.* **161**, 349–358 (2018). <https://doi.org/10.1016/j.petrol.2017.11.051>
- Lanetc, Z., Zhuravljov, A., Shapoval, A., Armstrong, R.T., Mostaghimi, P., 2022. Inclusion of microporosity in numerical simulation of relative permeability curves, In: Day 1 Mon, February 21, 2022. Presented at the International Petroleum Technology Conference, IPTC, Riyadh, Saudi Arabia, p. D012S111R003. <https://doi.org/10.2523/IPTC-21975-MS>
- Li, L., Li, B.: Implementation and validation of a volume-of-fluid and discrete-element-method combined solver in OpenFOAM. *Particuology* **39**, 109–115 (2018). <https://doi.org/10.1016/j.partic.2017.09.007>
- Mahani, H., Keya, A.L., Berg, S., Bartels, W.-B., Nasralla, R., Rossen, W.R.: Insights into the mechanism of wettability alteration by low-salinity flooding (LSF) in Carbonates. *Energy Fuels* **29**, 1352–1367 (2015). <https://doi.org/10.1021/ef5023847>
- Mahani, H., Keya, A.L., Berg, S., Nasralla, R.: Electrokinetics of carbonate/brine interface in low-salinity waterflooding: effect of brine salinity, composition, rock Type, and pH on ζ -potential and a surface-complexation model. *SPE J.* **22**, 53–68 (2017). <https://doi.org/10.2118/181745-PA>

- Masalmeh, S., Al-Hammadi, M., Farzaneh, A., Sohrabi, M., 2019. Low salinity water flooding in carbonate: screening, laboratory quantification and field implementation, In: Day 3 Wed, November 13, 2019. Presented at the Abu Dhabi International Petroleum Exhibition & Conference, SPE, Abu Dhabi, UAE, p. D031S094R001. <https://doi.org/10.2118/197314-MS>
- Maskari, N.S.A., Sari, A., Hossain, M.M., Saeedi, A., Xie, Q.: Response of non-polar oil component on low salinity effect in carbonate reservoirs: adhesion force measurement using atomic force microscopy. *Energies* **13**, 77 (2020). <https://doi.org/10.3390/en13010077>
- McAuliffe, C.D.: Crude-oil-water emulsions to improve fluid flow in an oil reservoir. *J. Petrol. Technol.* **25**, 721–726 (1973a). <https://doi.org/10.2118/4370-PA>
- McAuliffe, C.D.: Oil-in-water emulsions and their flow properties in porous media. *J. Petrol. Technol.* **25**, 727–733 (1973b). <https://doi.org/10.2118/4369-PA>
- Meng, W., Haroun, M.R., Sarma, H.K., Adeoye, J.T., Aras, P., Punjabi, S., Rahman, M.M., Al Kob-aisi, M., 2015. A Novel Approach of Using Phosphate-spiked Smart Brines to Alter Wettability in Mixed Oil-wet Carbonate Reservoirs. In: Presented at the Abu Dhabi international petroleum exhibition and conference, OnePetro. <https://doi.org/10.2118/177551-MS>
- Mohammadi, M., Nikbin-Fashkacheh, H., Mahani, H.: Pore network-scale visualization of the effect of brine composition on sweep efficiency and speed of oil recovery from carbonates using a photolithography-based calcite microfluidic model. *J Petrol Sci Eng* **208**, 109641 (2022). <https://doi.org/10.1016/j.petrol.2021.109641>
- Myint, P.C., Firoozabadi, A.: Thin liquid films in improved oil recovery from low-salinity brine. *Curr. Opin. Colloid Interface Sci.* **20**, 105–114 (2015). <https://doi.org/10.1016/j.cocis.2015.03.002>
- Namaee-Ghasemi, A., Ayatollahi, S., Mahani, H.: Pore-scale simulation of the interplay between wettability, capillary number, and salt dispersion on the efficiency of oil mobilization by low-salinity waterflooding. *SPE J.* **26**, 4000–4021 (2021). <https://doi.org/10.2118/206728-PA>
- Pourakabarian, A., Mahani, H., Niasar, V.: The impact of the electrical behavior of oil-brine-rock interfaces on the ionic transport rate in a thin film, hydrodynamic pressure, and low salinity waterflooding effect. *Coll Surf A: Physicochem Eng Aspects* **620**, 126543 (2021). <https://doi.org/10.1016/j.colsurfa.2021.126543>
- Pourakabarian, A., Mahani, H., Niasar, V.: Dynamics of electrostatic interaction and electrodiffusion in a charged thin film with nanoscale physicochemical heterogeneity: implications for low-salinity waterflooding. *Coll Surf A: Physicochem Eng Aspects* **650**, 129514 (2022). <https://doi.org/10.1016/j.colsurfa.2022.129514>
- Qiao, C., Li, L., Johns, R.T., Xu, J.: A mechanistic model for wettability alteration by chemically tuned waterflooding in carbonate reservoirs. *SPE J.* **20**, 767–783 (2015). <https://doi.org/10.2118/170966-PA>
- Raeini, A.Q., Blunt, M.J., Bijeljic, B.: Direct simulations of two-phase flow on micro-CT images of porous media and upscaling of pore-scale forces. *Adv. Water Resour.* **74**, 116–126 (2014). <https://doi.org/10.1016/j.advwatres.2014.08.012>
- Rapoport, L.A., Leas, W.J.: Properties of linear waterfloods. *J. Petrol. Technol.* **5**, 139–148 (1953). <https://doi.org/10.2118/213-G>
- Sanaei, A., Tavassoli, S., Sepehrnoori, K.: Investigation of modified Water chemistry for improved oil recovery: application of DLVO theory and surface complexation model. *Colloids Surf., A* **574**, 131–145 (2019). <https://doi.org/10.1016/j.colsurfa.2019.04.075>
- Scanziani, A., Singh, K., Bultreys, T., Bijeljic, B., Blunt, M.J.: In situ characterization of immiscible three-phase flow at the pore scale for a water-wet carbonate rock. *Adv. Water Resour.* **121**, 446–455 (2018). <https://doi.org/10.1016/j.advwatres.2018.09.010>
- Selem, A.M., Agenet, N., Gao, Y., Raeini, A.Q., Blunt, M.J., Bijeljic, B.: Pore-scale imaging and analysis of low salinity waterflooding in a heterogeneous carbonate rock at reservoir conditions. *Sci Rep* **11**, 15063 (2021). <https://doi.org/10.1038/s41598-021-94103-w>
- Shams, M., Singh, K., Bijeljic, B., Blunt, M.J.: Direct numerical simulation of pore-scale trapping events during capillary-dominated two-phase flow in porous media. *Transp Porous Med* **138**, 443–458 (2021). <https://doi.org/10.1007/s11242-021-01619-w>
- Shapoval, A., Haryono, D., Cao, J.L., Rahman, S.S.: Pore-scale investigation of the ion-tuned water effect on the surface properties of limestone reservoirs. *Energy Fuels* (2021). <https://doi.org/10.1021/acs.energyfuels.1c00382>
- Shapoval, A., Alzahrani, M., Xue, W., Qi, X., Rahman, S.: Oil-water interactions in porous media during fluid displacement: effect of potential determining ions (PDI) on the formation of in-situ emulsions and oil recovery. *J Petrol Sci Eng* **210**, 110079 (2022). <https://doi.org/10.1016/j.petrol.2021.110079>

- Shirazi, M., Farzaneh, J., Kord, S., Tamsilian, Y.: Smart water spontaneous imbibition into oil-wet carbonate reservoir cores: Symbiotic and individual behavior of potential determining ions. *J Molecul Liq* **299**, 112102 (2020). <https://doi.org/10.1016/j.molliq.2019.112102>
- Song, J., Wang, Q., Shaik, I., Puerto, M., Bikkina, P., Aichele, C., Biswal, S.L., Hirasaki, G.J.: Effect of salinity, Mg^{2+} and SO_4^{2-} on “smart water”-induced carbonate wettability alteration in a model oil system. *J. Colloid Interface Sci.* **563**, 145–155 (2020). <https://doi.org/10.1016/j.jcis.2019.12.040>
- Standnes, D.C., Austad, T.: Wettability alteration in chalk: 2. Mechanism for wettability alteration from oil-wet to water-wet using surfactants. *J. Petrol. Sci. Eng.* **28**, 123–143 (2000). [https://doi.org/10.1016/S0920-4105\(00\)00084-X](https://doi.org/10.1016/S0920-4105(00)00084-X)
- Tetteh, J.T., Cudjoe, S.E., Aryana, S.A., Barati Ghahfarokhi, R.: Investigation into fluid-fluid interaction phenomena during low salinity waterflooding using a reservoir-on-a-chip microfluidic model. *J Petrol Sci Eng* **196**, 108074 (2021). <https://doi.org/10.1016/j.petrol.2020.108074>
- Umar, A.A., Saaid, I.B.M., Sulaimon, A.A., Pilus, R.B.M.: A review of petroleum emulsions and recent progress on water-in-crude oil emulsions stabilized by natural surfactants and solids. *J. Petrol. Sci. Eng.* **165**, 673–690 (2018). <https://doi.org/10.1016/j.petrol.2018.03.014>
- Unsal, E., Broens, M., Armstrong, R.T.: Pore scale dynamics of microemulsion formation. *Langmuir* **32**, 7096–7108 (2016). <https://doi.org/10.1021/acs.langmuir.6b00821>
- Unsal, E., Rücker, M., Berg, S., Bartels, W.B., Bonnín, A.: Imaging of compositional gradients during in situ emulsification using x-ray micro-tomography. *J. Colloid Interface Sci.* **550**, 159–169 (2019). <https://doi.org/10.1016/j.jcis.2019.04.068>
- Visser, J.: On Hamaker constants: a comparison between Hamaker constants and Lifshitz-van der Waals constants. *Adv. Coll. Interface. Sci.* **3**, 331–363 (1972). [https://doi.org/10.1016/0001-8686\(72\)85001-2](https://doi.org/10.1016/0001-8686(72)85001-2)
- Vogel, H.-J., Tölke, J., Schulz, V.P., Krafczyk, M., Roth, K.: Comparison of a lattice-boltzmann model, a full-morphology model, and a pore network model for determining capillary pressure-saturation relationships. *Vadose Zone Journal* **4**, 380–388 (2005). <https://doi.org/10.2136/vzj2004.0114>
- Yousef, A.A., Al-Saleh, S.H., Al-Kaabi, A., Al-Jawfi, M.S.: Laboratory investigation of the impact of injection-water salinity and ionic content on oil recovery from carbonate reservoirs. *SPE Reservoir Eval. Eng.* **14**, 578–593 (2011). <https://doi.org/10.2118/137634-PA>
- Yuan, W.: Water-sensitive characterization and its controlling factors in clastic reservoir: a case study of Jurassic Ahe Formation in Northern tectonic zone of Kuqa depression. *Petrol. Res.* **5**, 77–82 (2020). <https://doi.org/10.1016/j.ptlrs.2019.07.002>
- Zhang, P., Tweheyo, M.T., Austad, T.: Wettability alteration and improved oil recovery by spontaneous imbibition of seawater into chalk: impact of the potential determining ions Ca^{2+} , Mg^{2+} , and SO_4^{2-} . *Coll. Surf., A* **301**, 199–208 (2007). <https://doi.org/10.1016/j.colsurfa.2006.12.058>

Publisher's Note Springer Nature remains neutral with regard to jurisdictional claims in published maps and institutional affiliations.